Supplementary Information

Lateral Sorting of Chiral Nanoparticles Using Fano-Enhanced Chiral Force in the visible region

Tun Cao* and Yimei Qiu

Department of Biomedical Engineering, Dalian University of Technology, Dalian 116024, China.
E-mail: caotun1806@dlut.edu.cn

Session 1. Optical forces in the dipolar system

A chiral particle whose dimensions are significantly smaller than the spatial change of the surrounding harmonic electromagnetic (EM) field can be described as a pair of interacting electric $\mathrm{P} = \mathrm{Re}[\mathbf{p}(\mathbf{r})\mathbf{e}^{-i\omega t}]$ and magnetic $\mathbf{M} = \mathrm{Re}[\mathbf{m}(\mathbf{r})\mathbf{e}^{-i\omega t}]$ dipolar moments, in which the chiral particle subjected to the monochromatic EM-field generates the moments of $\mathbf{p}$ and $\mathbf{m}$ associate with both the local electric $\mathbf{E}$ and magnetic $\mathbf{H}$ fields at the target particle that are expressed as [77]

$$\begin{pmatrix} \mathbf{p} \\ \mathbf{m} \end{pmatrix} = \begin{pmatrix} \alpha\varepsilon_{\mathrm{d}} & i\chi\sqrt{\varepsilon_{\mathrm{d}}\mu_{\mathrm{d}}} \\ -i\chi\sqrt{\varepsilon_{\mathrm{d}}\mu_{\mathrm{d}}} & \beta\mu_{\mathrm{d}} \end{pmatrix} \times \begin{pmatrix} \mathbf{E} \\ \mathbf{H} \end{pmatrix} \tag{s1}$$

where ε_{d} and μ_{d} are the permittivity and permeability of the surrounding media, respectively, electric α, magnetic β, and mixed electric-magnetic χ dipole polarizabilities are complex scalars. Notably, the sign (+, -) of χ polarizability is closely related to the handedness of enantiomers. It should be noted that the α and β polarizabilities are always the same during enantiomeric variations as they are quadratic forms of the electric and magnetic dipoles, respectively [13,77]. Therefore, one of our purposes is to discriminate the effect of the sign change of χ on the optical forces for the chiral dipoles. For a nanosphere, the polarizabilities of α, β and χ can be directly shown as [6],

$$\alpha = 4\pi R^3 \frac{(\varepsilon_{\mathrm{r}}-1)(\mu_{\mathrm{r}}+2)-\kappa^2}{(\varepsilon_{\mathrm{r}}+2)(\mu_{\mathrm{r}}+2)-\kappa^2} \tag{s2}$$

$$\beta = 4\pi R^3 \frac{(\mu_{\mathrm{r}}-1)(\varepsilon_{\mathrm{r}}+2)-\kappa^2}{(\varepsilon_{\mathrm{r}}+2)(\mu_{\mathrm{r}}+2)-\kappa^2} \tag{s3}$$

$$\chi = 12\pi R^3 \frac{\kappa}{(\varepsilon_{\mathrm{r}}+2)(\mu_{\mathrm{r}}+2)-\kappa^2} \tag{s4}$$

$\varepsilon_{\mathrm{r}} = \varepsilon / \varepsilon_{\mathrm{d}}$ and $\mu_{\mathrm{r}} = \mu / \mu_{\mathrm{d}}$ are the relative permittivity and permeability with respect to the surrounding media, (ε, μ) gives the refractive index n of the nanosphere, κ determines the chirality of the sphere that links to the effective refractive index difference $n_{\pm} = n \pm \kappa$ between left (-) and right (+) handed circularly polarized waves, and it measures the level of handedness of chiral molecules. The imaginary ($\mathrm{Im}(\kappa)$) and real parts ($\mathrm{Re}(\kappa)$) of κ are related to the chiral response and optical rotation, respectively. R is the radius of the nanoparticle. A detailed derivation of polarizabilities (Eqs.(s2)-(s4)) can be found in the Appendix of Ref.[6].

The time-averaged optical force $\mathbf{F}$ exerted on a chiral particle can be expressed from the Lorentz force law [13,77],

$$\mathbf{F} = \frac{1}{2}\mathrm{Re}\left[(\mathbf{p}\cdot\nabla)\mathbf{E}^{*} + (\mathbf{m}\cdot\nabla)\mathbf{H}^{*} - i\omega\mu_{\mathrm{d}}\mathbf{p}\times\mathbf{H}^{*} + i\omega\varepsilon_{d}\mathbf{m}\times\mathbf{E}^{*}\right] \tag{s5}$$

It should be pointed out that, herein we do not consider the terms stemming from self-interactions of the dipole that plays a role in producing the recoil force. The $\mathbf{F}$ can then be presented as a sum of a non-chiral ($\mathbf{F}_{\alpha,\beta}$) and chiral gradient forces ($\mathbf{F}_{\chi}$) associated with (α, β) and χ polarizabilities, respectively.

$$\mathbf{F} = \mathbf{F}_{\alpha,\beta} + \mathbf{F}_{\chi} \tag{s6}$$

By placing the dipolar moments ($\mathbf{p}$, $\mathbf{m}$) shown in Eq. (s1) into Eq. (s5), the $\mathbf{F}_{\alpha,\beta}$ and $\mathbf{F}_{\chi}$ can be both divided into reactive and dissipative constituents, respectively, which consist of the real and imaginary parts of the α, β, and χ polarizabilities:

$$\mathbf{F}_{\alpha,\beta}^{\mathrm{reac}} = \mathrm{Re}[\alpha]\nabla W_{\mathrm{E}} + \mathrm{Re}[\beta]\nabla W_{\mathrm{H}} \tag{s7}$$

$$\mathbf{F}_{\alpha,\beta}^{\mathrm{diss}} = \frac{\omega\,\mathrm{Im}[\alpha]\boldsymbol{\Pi}_{\mathrm{O}}^{(\mathrm{E})}}{c^{2}} + \frac{\omega\,\mathrm{Im}[\beta]\boldsymbol{\Pi}_{\mathrm{O}}^{(\mathrm{H})}}{c^{2}} \tag{s8}$$

$$\mathbf{F}_{\chi}^{\mathrm{reac}} = \mathrm{Re}[\chi]\cdot\frac{c}{\omega}\nabla\mathbf{C} \tag{s9}$$

$$\mathbf{F}_{\chi}^{\mathrm{diss}} = \mathrm{Im}[\chi]\cdot\frac{2}{c}\left(\Phi - \frac{\nabla\times\Pi}{2}\right) \tag{s10}$$

where $W_{\mathrm{E}} = \frac{\varepsilon_{\mathrm{d}}}{4}\|\mathbf{E}\|^{2}$ and $W_{\mathrm{H}} = \frac{\mu_{\mathrm{d}}}{4}\|\mathbf{H}\|^{2}$ are the energy densities of both electric and magnetic field, respectively, $\boldsymbol{\Pi}_{\mathrm{O}}^{(\mathrm{E})} = \Pi - \frac{\nabla\times\Phi_{\mathrm{E}}}{2\omega\mu_{\mathrm{d}}}$ and $\boldsymbol{\Pi}_{\mathrm{O}}^{(\mathrm{H})} = \Pi - \frac{\nabla\times\Phi_{\mathrm{H}}}{2\omega\varepsilon_{\mathrm{d}}}$ are for both electric and magnetic orbital parts of the Poynting vector $\Pi = \frac{\mathrm{Re}\left[\mathbf{E}\times\mathbf{H}^{*}\right]}{2}$, respectively.

$K=\frac{\mathrm{Im}\left[\mathbf{E}\cdot\mathbf{H}^{*}\right]\omega}{2c^{2}}$ is the chirality density of the field and Φ is the flow of chirality. The flow of the chirality is determined by the electric and magnetic field ellipticities:

$$\Phi=\frac{\omega\left(\varepsilon_{\mathrm{d}}\Phi_{\mathrm{E}}+\mu_{\mathrm{d}}\Phi_{\mathrm{H}}\right)}{2} \tag{s11}$$

where $\Phi_{\mathrm{E}}=-\frac{1}{2}\mathrm{Im}\left[\mathbf{E}\times\mathbf{E}^{*}\right]$ and $\Phi_{\mathrm{H}}=-\frac{1}{2}\mathrm{Im}\left[\mathbf{H}\times\mathbf{H}^{*}\right]$.

Session 2. Fano formula fitting to the transmittance spectrum simulated through FDTD method

In Fig.S1(a), the Fano formula is expressed as [44],

$$T=(\frac{q_n^2-1}{\varepsilon_n^2+1})+(\frac{2q_n\varepsilon_n}{\varepsilon_n^2+1})+1=\frac{(\varepsilon_n+q_n)^2}{\varepsilon_n^2+1} \tag{s12}$$

which is a superposition of the Lorentzian function of the discrete level ($(\frac{q_n^2-1}{\varepsilon_n^2+1})$) with a flat continuous background (1), where $(\frac{2q_n\varepsilon_n}{\varepsilon_n^2+1})$ represents the mixing between the Lorentzian function and flat continuous background. By considering the amplification factor (F_n) and displacement (A_m) of Fano formula along the longitudinal axis, Eq.(s12) is rewritten as,

$$T=A_m+F_n\frac{(\varepsilon_n+q_n)^2}{\varepsilon_n^2+1} \tag{s13}$$

where $\varepsilon_n=\frac{2(\omega-\omega_n)}{\Gamma_n}$, Γ_{n} the width of the autoionized state, ω_n the resonant frequency of $\mathrm{P_n}$ mode, q_n the phenomenological shape parameters, A_m and F_n the constant factors.In Fig. S1(b)-(c), we fit the transmittance of both the symmetric double split-ring resonator (SDSRR) and asymmetric double split-ring resonator (ADSRR) using the single FR lineshape in Eq. (s14) [43,44] and double FR lineshape in Eq.(s15) [s1], respectively,

$$T=A_0+F_3\frac{(\varepsilon_3+q_3)^2}{1+\varepsilon_3^2} \tag{s14}$$

$$T=A_1+F_4\frac{(\varepsilon_4+q_4)^2}{1+\varepsilon_4^2}+F_5\frac{(\varepsilon_5+q_5)^2}{1+\varepsilon_5^2} \tag{s15}$$

where $\varepsilon_3=\frac{2(\omega-\omega_3)}{\Gamma_3}$, $\varepsilon_4=\frac{2(\omega-\omega_4)}{\Gamma_4}$, $\varepsilon_5=\frac{2(\omega-\omega_5)}{\Gamma_5}$. With the parameters shown in Table S1, the calculated transmittances using Eqs. (s14) and (s15) approximately reproduce the transmittance simulated by the finite difference time domain (FDTD) method.

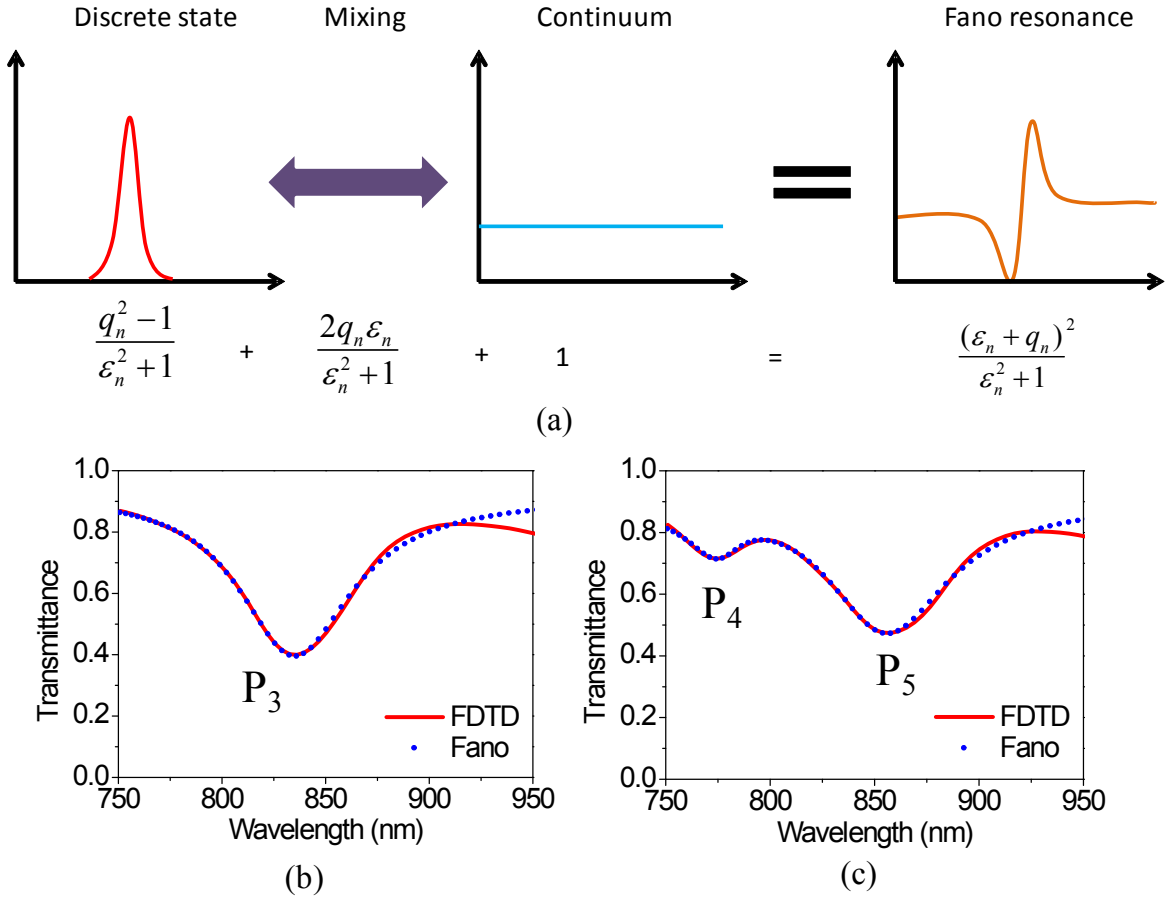

Fig.S1. (a) Demonstration of Fano lineshape as a superposition of the Lorentzian line shape of the discrete level with a flat continuous background. (b) FDTD simulation of the transmittance spectrum (red solid) of SDSRR and best-fits to the Fano lineshape using Eq.(s14) (blue dot). (c) FDTD simulation of the transmittance spectrum (red solid) of ADSRR and best-fits to the Fano lineshape using Eq.(s15) (blue dot).

Table S1: Fano formula fitted parameters of the transmittances for the different double split-ring resonators.

Mode	ω_n	Γ_n	q_n	Q_n
P_3	360.8THz	26.9THz	-0.3957	13
P_4	388.3THz	11.76THz	0.173	33
P_5	351.5THz	23.3THz	-0.0381	15

[s1] Y. Ma, Z. Li, Y. Yang, R. Huang, R. Singh, S. Zhang, J. Gu, Z. Tian, J. Han, and W. Zhang, *Opt. Mater. Express*, 2011, **1**, 391–399.

Session 3. The effect of structure's geometry on the lateral forces for the enantiomers in the air.

To understand the effect of structure's geometry on the lateral force, we calculate the spectra of the $\mathbf{F}^x$ (left column) and $\mathbf{F}^y$ (right column) exerted on the chiral nanoparticles placed 10 nm above ADSRR by varying w from 25 nm to 40 nm with the fixed parameters of $\alpha = 10^0$, $\beta_1 = 170^0, \beta_2 = 140^0$ (Fig. S2(a)), varying α from 5^0 to 20^0 with the fixed parameters of $w = 30$ nm, $\beta_1 = 170^0, \beta_2 = 140^0$ (Fig. S2(b)), and varying β_1/β_2 from 1.1 to 1.4 with the fixed parameters of $\alpha = 10^0$ and $w = 30$ nm (Fig. S2(c)). As can be seen, the two total lateral forces ($\mathbf{F}^x$ and $\mathbf{F}^y$) present the most pronounced change by the enantiomeric pair with the parameters of $w = 30$ nm, $\alpha = 10^0$, $\beta_1 = 170^0, \beta_2 = 140^0$. In Fig. S2(d), we calculate the spectra of $\mathbf{F}^x$ (left column) and $\mathbf{F}^y$ (right column) by changing the gap between the two nested SRRs. Mainly, we vary the R_i from 150 nm to 165 nm while fixing the other parameters. It shows that the total lateral forces become more significant as increasing R_i (namely reducing the gap). This is because the proximity between the inner and outer SRRs leads to mode hybridization and the stronger resonances, which can offer substantial field gradient in the x-y plane [2,11, 42]. The best performance of the lateral forces variations is with $R_i = 165$ nm corresponding to the gap width of 15 nm, whereas this is smaller than the diameter of the chiral particles ($d = 20$ nm). To match the size of the chiral particles while maintaining a significant enhancement of the lateral force, herein we choose the width of a plasmonic gap as 20 nm.

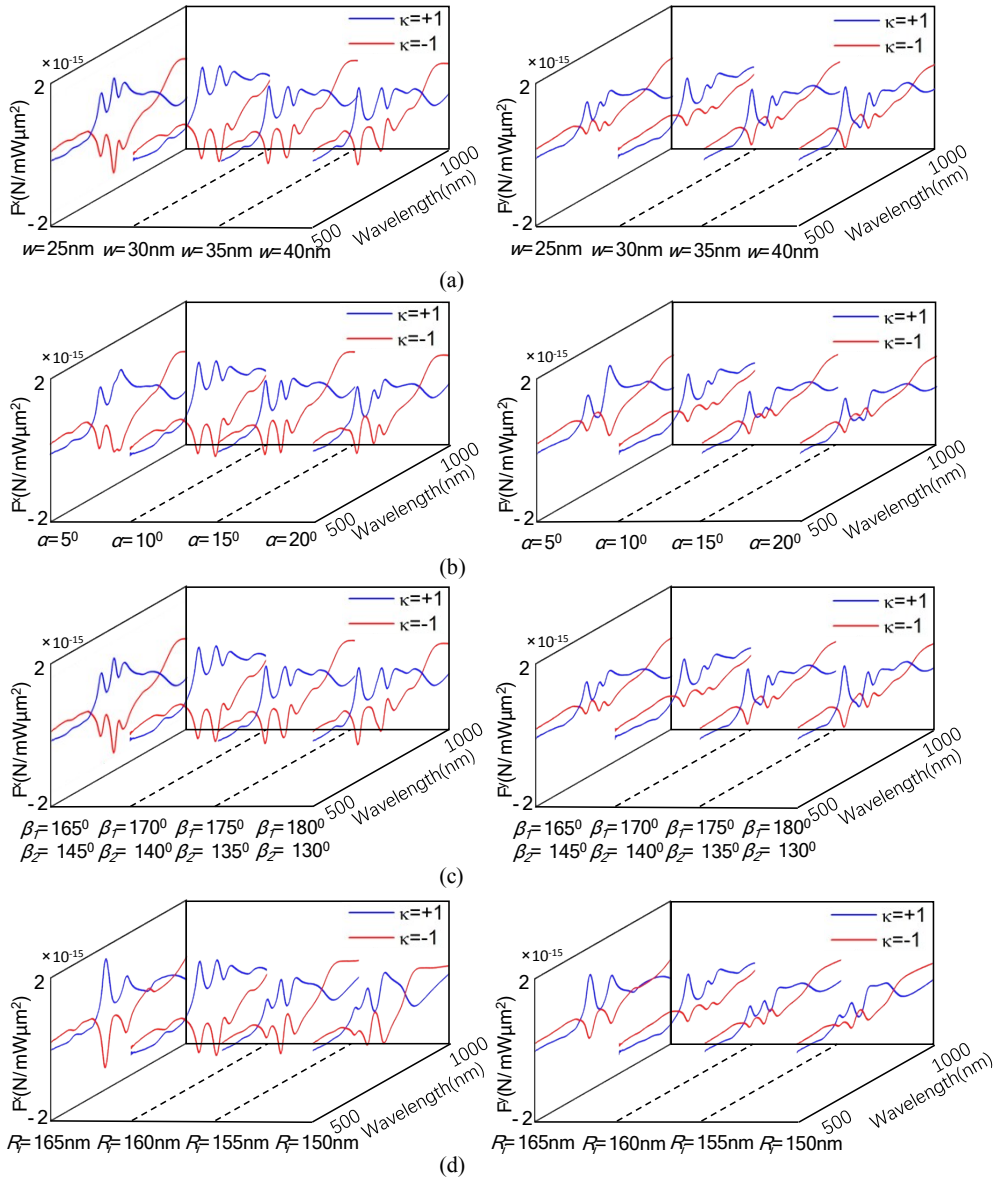

Fig. S2. Spectra of the lateral optical forces exerted on the enantiomers placed 10 nm above the ADSRR with (a) w from 25 nm to 40 nm, α =10^0, β_1=170^0,β_2= 140^0, (b) α from 5^0 to 20^0, w =30 nm, β_1=170^0,β_2= 140^0, (c) β_1/β_2 from 1.1 to 1.4, α =10^0 , w =30 nm, (d) R_i from 150 nm to 165 nm, R_0 = 210 nm, α =10^0 , w =30 nm, β_1= 170^0, β_2= 140^0.The total lateral forces along both the x- and y-axes are shown in the left- and right-columns, respectively.

In Fig. S3(a), we present a comparison of transmittances between the square SDSRR (solid blue line) and square ADSRR (solid red line). Our results show that the P_6 mode at λ=830 nm can be split into two distinct resonance modes at λ = 768 (denoted as P_7) and 861 nm (indicated as P_8) by breaking the symmetry of the inner square SRR. In Fig. S3(b), a ratio of K/K_{CPL} is calculated to evaluate the enhancement of optical chirality intensity for both the square SDSRR and square ADSRR. As can be seen, the distributions of K/K_{CPL} in the square DSRR follow the

similar trend as the K/K_{CPL} in the circular DSRR (Fig.2). The geometries of the square DSRRs are determined from the circular DSRRs.

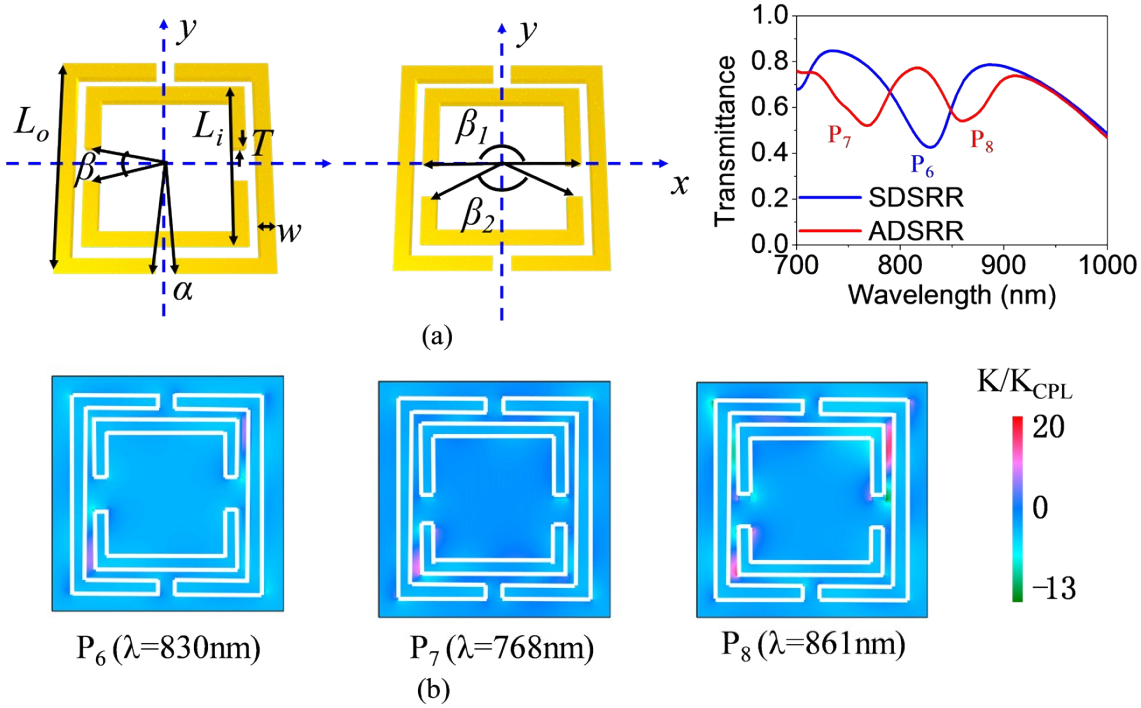

Fig.S3. (a) A comparison of the transmittances between the square SDSSR and square ADSRR, where L_i = 320 nm, L_0 = 420 nm, α =10^0, β=25^0, β_1=180^0,β_2= 130^0, w=30 nm, and T= 30 nm. (b) Enhancements of the optical chirality intensity K/K_{CPL} at λ= 830nm (P_6 mode, left column), λ = 768 nm (P_7 mode, central column), and λ = 861 nm (P_8 mode, right column).

Session 4. Trapping potentials for the enantiomers with the 250 mW LCP incidence in air.

To compensate for the delocalization and prevent the nanoparticle from escaping, the trapping confinement needs to satisfy $U_B > 10\ k_BT$ by either further focusing the trapping laser beam or by increasing the local laser intensity on the specimen [41,79]. Figure S4 depicts U_B of the paired enantiomers by increasing LCP light power to 250 mW. Figure S4(a) presents 2D U_B on the right-handed chiral particle (R =10 nm, κ=+1) placed 10 nm above the plasmonic aperture. Figure S4(b) demonstrates the same U_B on the left-handed chiral specimen (R=10 nm, κ=-1). Figure S4(c) shows 1D U_B along the diagonal direction across the plasmonic aperture (α plane in Fig. S4(a)-(b)) for the enantiomeric pair. With the LCP illumination, the same gap offers U_B as deep as −14 k_BT for the right-handed enantiomer, while for the left-hand specimen the U_B is positive (U_B = +13 k_BT) at the same position. The significant variations in the sign and magnitude of optical forces for the enantiomeric pair lead to a drastic difference in their U_B.

Such a distinct U_B stably captures the right-handed enantiomer around the aperture, while acting as a potential barrier to repel the left-handed enantiomer. By just switching the incidence polarization to right circularly polarization (RCP), we may trap the other handedness. Then the same trapping potential (U_B=−14k_BT) for the right-handed enantiomer could apply to the left-handed enantiomer.

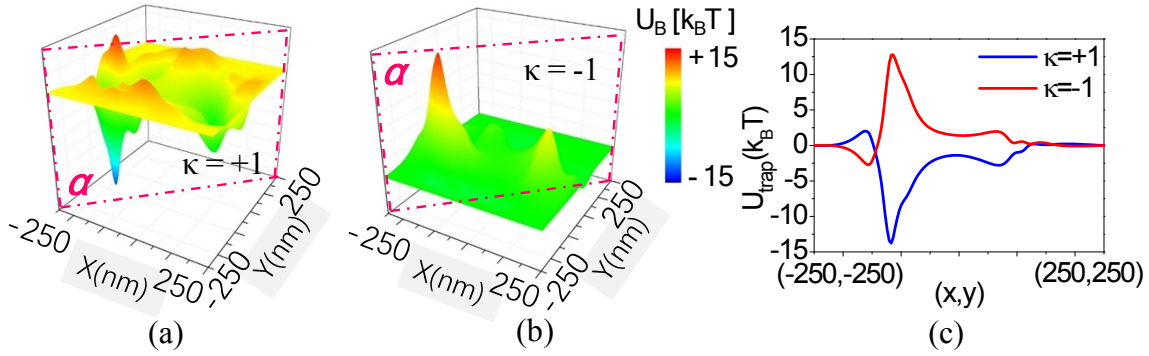

Fig. S4. Trapping potentials for the paired enantiomers (R= 10 nm, κ = ±1) with 250 mW LCP incidence in air. 2D trapping potentials for (a) right-handed enantiomer and (b) left-handed enantiomer at 10 nm away from the aperture. (c) 1D trapping potentials across the diagonal direction of the aperture (α plane) for both right-handed (κ =+1, blue line) and left-handed (κ =-1, red line) enantiomers. The resonance wavelength is at λ= 774 nm (P_4 mode)

Session 5. The effect of chirality parameter and incident power on the transverse forces for the enantiomers in the air.

So far, we take κ = ±1 as an example to illustrate the crucial role of the Fano resonance for the enhancement of the lateral chiral force. The same design can also obtain an enantioselection of chiral specimen with κ = ±0.7 (Fig. S5 (a)); moreover, herein the incident power is 25 mW that is much lower than 100mW employed in Ref. [2]. By enlarging the input power to 75 mW, a significant variation of the total transverse force by the enantiomeric pair with a smaller κ = ±0.3 can be attained (left and central columns of Fig. S5(b)). These result in separations of the chiral particles with the opposite handedness for both of the situations. In the right column of Fig. S5, we show the dynamic simulation of the stability of sub-10 nm enantiomeric pairs by observing time sequences of the particles' movements above the plasmonic aperture at λ=774 nm (P_4 mode). The chiral particles are tracked with "nm" accuracy in the x-y plane. The powers of LCP illumination are 25 mW and 75 mW for the chiral particles with κ = ±0.7 and ±0.3, respectively. A trajectory of the chiral nanoparticle with κ > 0 is shown by the blue line. On the contrary, the chiral nanoparticle with the opposite handedness (κ<0) follows the different direction of motion (indicated by the red line).

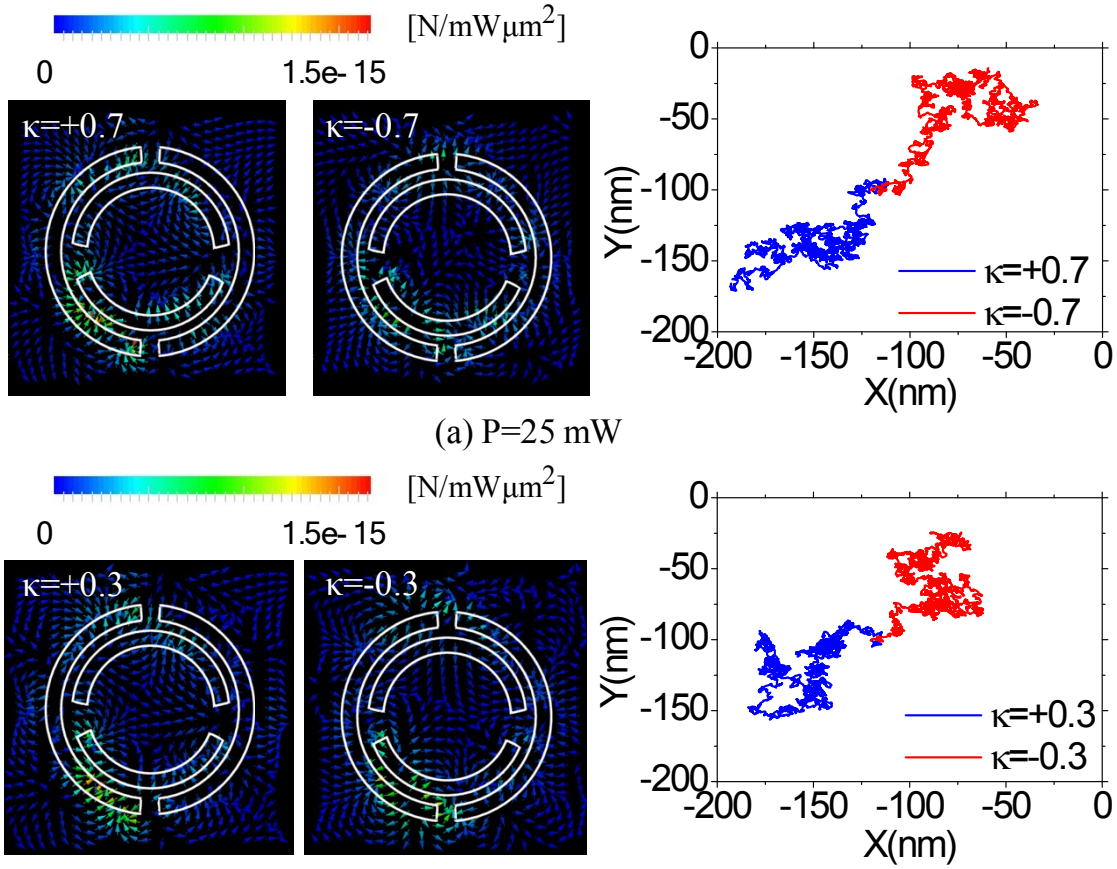

Fig. S5. The transverse total forces **F** acting on the paired enantiomers with R=10 nm for (a) $\kappa=\pm0.7$ under 25 mW LCP light, and (b) $\kappa=\pm0.3$ under 75 mW LCP light. Left column: **F** with $\kappa>0$; central column: **F** with $\kappa<0$; right column: the stability of the enantiomeric pair, where the blue and red solid lines represent the 0.1 ms trajectories of the chiral particles with $\kappa>0$ and $\kappa<0$, respectively. The particles are placed 10 nm above the aperture of the ADSRR. The white solid lines outline the structure's geometry, and the color and direction of the arrows represent the magnitude and direction of the forces, respectively. The resonance wavelength is at λ= 774 nm (P_4 mode).

Session 6. Optical separation of the paired enantiomers in water.

Figure S6 depicts the optical potentials (U_B) of the paired enantiomers with a left circularly polarized (LCP) incidence, where the enantiomers are at 10 nm away from the surface of ADSRR in the water, the power of the LCP incidence is 700 mW, and the resonance wavelength is λ=774 nm (P_4 mode). Figure S6(a) presents the two dimensional (2D) U_B on the right-handed chiral particle (R=10 nm, κ=+1). Figure S6(b) demonstrates the same U_B on the left-handed chiral specimen (R=10 nm, κ=-1). Figure S6(c) shows the one dimensional (1D) U_B along the diagonal direction across the plasmonic aperture (α plane) for the enantiomeric pair. With the LCP illumination, the same aperture offers U_B as deep as $-11\ k_BT$ for the right-handed enantiomer, while for the left-hand specimen the U_B is positive (U_B=+11.5 k_BT) at the identical position. Such a distinct U_B stably captures the right-handed enantiomer around the aperture, while acting as a potential barrier to repel the left-handed enantiomer. By just switching the incidence polarization to right circularly polarization (RCP), we may trap the other handedness. Then the same trapping potential (U_B=−11 k_BT) for the right-handed enantiomer could apply to the left-handed enantiomer.

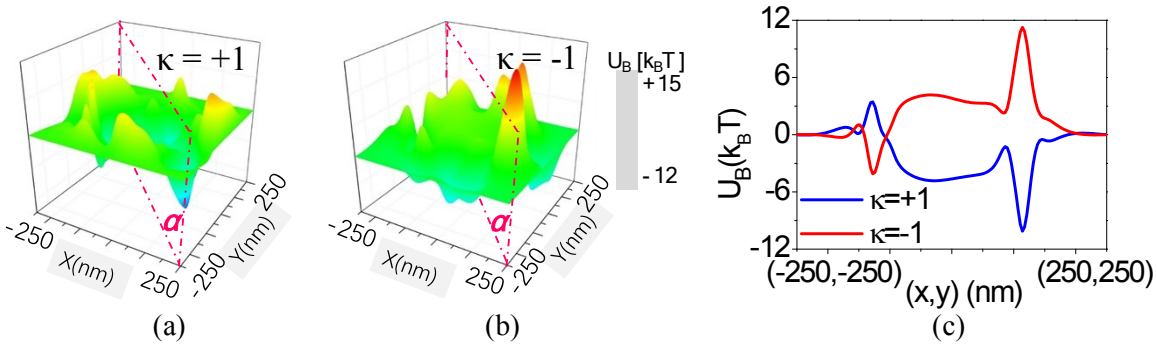

Fig. S6. Trapping potentials for the paired enantiomers (R= 10 nm) with 700 mW LCP incidence in water. 2D trapping potentials for (a) right-handed enantiomer and (b) left-handed enantiomer at 10 nm above the nanoaperture. (c) 1D trapping potentials across the diagonal direction of the aperture (α plane) for both right-handed (κ =+1, blue line) and left-handed (κ =-1, red line) enantiomers.